

UCSF

UC San Francisco Electronic Theses and Dissertations

Title

Neutrophils actively swell to potentiate rapid migration

Permalink

<https://escholarship.org/uc/item/4rr9086f>

Author

Nagy, Tamas Laszlo

Publication Date

2023

Peer reviewed|Thesis/dissertation

Neutrophils actively swell to potentiate rapid migration

by
Tamas Nagy

DISSERTATION
Submitted in partial satisfaction of the requirements for degree of
DOCTOR OF PHILOSOPHY

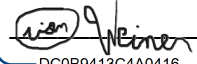
in

Biological and Medical Informatics

in the

GRADUATE DIVISION
of the
UNIVERSITY OF CALIFORNIA, SAN FRANCISCO

Approved:

DocuSigned by:

DC0B9413C4A0416... Orion Weiner
Chair

DocuSigned by:

DocuSigned by: 9D... Fred Chang


DocuSigned by: 94... Lily Jan


DocuSigned by: 94... Alan Verkman
0147600CEA2648E...

Committee Members

Copyright 2023

by

Tamas Laszlo Nagy

Acknowledgments

Orion always says that a PhD takes a village and it could not be more true in my case. I came to UCSF almost 8 years ago now and I can say that these years have been a time of incredible growth for me. I believe its primarily due to the fantastic community that we have here. Folks are incredibly kind, open, and generous with their time and resources. Perhaps most importantly, theyre willing to suspend their disbelief for a moment and entertain the truly crazy ideas that a young student might have. I think the most important thing I have learned in my time here is what types of questions that I like to pursue; what kind of science I find exciting. And the willingness of my mentors and colleagues over the years to actively listen, but also to challenge me to flesh out my ideas has gone a long way to help me develop my heuristics for how I like to think about science.

First and foremost, Orion has been instrumental in this learning process. He gave me the time and space to make the boneheaded mistakes I needed to make to learn and develop. He is incredibly good at the yes and approach to science (a la Uri Alon) that let me explore some wild ideas that got me out of local minima. His ability to look at problems with fresh eyes and a positive attitude even when I brought disappointing news for many weeks in a row is aspirational. With Orion, it was always us versus the problem and I cannot express how important that was for me to build my confidence as a scientist. And finally, I think the lab environment that Orion has crafted with incredibly bright and helpful people working on disparate problems helped me keep the big picture in mind throughout my PhD.

The lab culture was a major part of my decision to join. Folks like Anne Pipathsouk and Brian Graziano were instrumental in teaching the system and their patience and experience were key to get me up and running. I was also very lucky that 2 other students, Rachel Brunetti and Derek Britain, joined at the same time as me and we were able to share in the PhD journey together. I also learned an incredible amount from the students who came before and those who joined after. Jason Town and Jack Strickland both joined after me, but my experience wouldnt have been the same without them. It was helpful to have others who were also interested in more quantitative image analysis to bounce ideas off and keep those skills sharp. Finally, the lab has now completely turned over since I joined, but its reassuring to see that the culture is similarly helpful, creative, fun and irreverent. The lab is in good hands.

But the ecosystem at UCSF is far larger than just the lab. I met amazing people through my program and have made what I hope are lifelong friendships. Folks like Alex Wolff, David Bauer, Nadja Kern, and many more have opened my eyes to so many new experiences and they inspired me to be better at science and at life. I am thankful to have made such a rich network of friends and colleagues who are now spread across the globe doing incredible work in a myriad of companies, universities and institutions. I want to thank Martin Kampmann for taking me on for an extended rotation. Many of the skills I developed with him were vital to the direction of my PhD. I also want to thank Fred Chang, Lily Jan, Alan Verkman, Hana El-Samad, and Wallace Marshall for their contributions to helping me hone my project during my qualifying exam and committee meeting. It takes a time and many false starts

to get a project streamlined and their balance of excitement, engagement, and demand for rigor was essential to this story.

Lastly, My family has been key to my experience in graduate school. My parents taught me so much about approaching the world with an open mind and they cultivated my scientific curiosity from a young age and let me run wild with it. And my long-term partner and now wife, Andrea Eastes, has been there through all of it. The highs. The lows. She has listened to me, challenged me, and helped me develop as a scientist and human. She has made this experience so much richer. I will be forever grateful that she shared this journey with me.

I was fortunate to have a village populated with folks who made my PhD possible. It has been transformative to me and my scientific journey. Heres to the next chapter.

Contributions

Chapter 1 is a modified version of:

Nagy, T. L., Strickland, J. D. & Weiner, O. D. Neutrophils actively swell to potentiate rapid migration. bioRxiv 2023.05.15.540704 (2023) doi:10.1101/2023.05.15.540704

and was written by Tamas Nagy, Jack Strickland, and Orion Weiner.

Abstract

Neutrophils actively swell to potentiate rapid migration

by

Tamas Laszlo Nagy

Neutrophils transform from a non-motile quiescent phenotype to rapidly moving amoeboid one when activated by chemoattractants. They are known to tune their properties to facilitate migration towards sites of injury or infection in the body. While the cytoskeletal changes cells adopt to enhance migration are well appreciated, much less is known about the hydrodynamic adaptations. Here, we measure single cell volumes during chemoattractant-induced neutrophil spreading and migration and find that the cells show a biphasic volume response. The cells first lose volume during spreading and they rapidly swell in volume within 15 minutes and this correlates with increased movement velocities. We leverage the power of genome-wide forward genetic screening to identify a volume regulatory network that the cells use to perform this swelling in response to chemoattractant. We then confirm that inhibition of this volume network is sufficient to completely block the swelling and leads to substantial velocity defects. Exogenously swelling of the cells with a mild hypoosmotic

shock is sufficient to rescue the velocity defect suggesting that swelling is key to potentiating cell migration in response to chemoattractants.

Contents

1	Neutrophils actively swell to potentiate rapid migration	1
1.1	Abstract	1
1.2	Results	4
1.3	Discussion	16
1.4	Materials and methods	20
	Bibliography	39

List of Figures

1.1	Fluorescence exclusion assay for measuring neutrophil volume during chemokinesis	5
1.2	Chemoattractant stimulation elicits competing volume responses in primary human neutrophils	6
1.3	Genome-wide screen identifies regulators of chemoattractant-induced cell swelling	9
1.4	Mechanistically separating chemoattractant versus motility-based volume changes	13
1.5	The chemoattractant-driven volume gain is necessary and sufficient for rapid cell migration following stimulation	15
1.6	Validation of the Fluorescence eXclusion Microscopy pipeline	35
1.7	Validation of buoyant density assay	36
1.8	Additional validation of swelling screen hits	37
1.9	Additional validation of motility phenotypes	38

List of Tables

1.1	Chemoattractant-induced swelling genome-wide CRISPR KO screen hits . . .	19
1.2	Volunteer Demographic Information	20
1.3	Guides used to make single gene knockouts in HL-60s	20

Chapter 1

Neutrophils actively swell to potentiate rapid migration

Tamas L Nagy, Jack D Strickland, Orion D Weiner

1.1 Abstract

Eukaryotic cell migration requires directed protrusion of the plasma membrane. While the role of actin polymerization in generating protrusive forces is well appreciated, we have a more limited understanding of the role of transmembrane water flow in cell motility. We investigate water influx-based migration in neutrophils, which undergo directed movement to sites of injury and infection. Chemoattractant exposure increases cell volume and potentiates neutrophil migration, but the causal link between these processes is not known. By measuring

single cell volumes in primary human neutrophils, we find that chemoattractant induces a biphasic volume response with spreading-mediated volume loss followed by an increase in both cell volume and migratory speed. Using a genome-wide CRISPR screen, we identify the regulators of the chemoattractant-induced neutrophil swelling, including PI3K-gamma, CA2, NHE1 and AE2. Through NHE1 inhibition in primary human neutrophils, we show that cell swelling is both necessary and sufficient for rapid migration following chemoattractant stimulation. Our data demonstrate that cell swelling complements cytoskeletal inputs for chemoattractant-induced rapid cell migration.

Introduction

Following chemoattractant exposure, neutrophils dramatically change their shape and movement. From a resting spherical shape, stimulated neutrophils polarize their actin assembly and actomyosin contractility to direct their movement to sites of injury and infection [25, 43, 52]. Actin cytoskeletal rearrangements are not the only modulators of cell shape and movement. Chemoattractant stimulation also initiates water influx, eliciting an approximately 15% increase in cell volume [17]. In contrast to the well-established role of the actin cytoskeleton in neutrophil movement, the role of water influx in chemoattractant-stimulated migration is poorly understood.

Directed water influx has previously been shown to participate in cell movement, particularly in the context of confined environments. In 1D confinement, directed water influx can

power cell migration even in the absence of the actin cytoskeleton [47]. Hypoosmotic shocks, which force water into the cytoplasm, have been shown to enhance neutrophil chemotaxis through nitrocellulose filters in vitro [40]. Here we investigated whether water influx is also relevant for unconfined 2D migration where actin polymerization is thought to dominate [23, 32]. There is growing appreciation that cell volume is tightly coupled to cell morphogenesis and mechanics [50], but whether cells actively manipulate water fluxes to potentiate their motility is unknown.

Here we leverage recent advances in measuring the volume of single cells [4, 55] to reveal the competing volume responses downstream of chemoattractant stimulation in human primary neutrophils. As the cells go from spherical to spread in response, they lose volume (as reported in other cell types by Venkova and colleagues [50]), but as they start migrating they then show a robust, sustained volume increase. We perform a genome-wide CRISPR screen to identify the mediators of this chemoattractant-induced cell swelling. By leveraging these regulators, we show that cell swelling is necessary and sufficient for the potentiation of cell migration following chemoattractant stimulation.

1.2 Results

Chemoattractant stimulation elicits competing volume responses in primary human neutrophils

Neutrophils are a powerful system to study the biophysical demands of cell motility, as they acutely initiate rapid migration following stimulation with chemoattractant. Neutrophils normally exist in a quiescent non-motile state [30]. Upon exposure to chemoattractants, neutrophils respond with large-scale morphological changes [7, 43] and a dramatic increase in motility [29].

To probe the role of osmotics in chemoattractant-stimulated morphogenesis and movement (Fig 1.1A; Fig 1.6A-E), we adapted the single cell volume measurement technique, Fluorescence eXclusion Microscopy (FxM) [4] to primary human neutrophils. This assay enables us to accurately measure absolute cell volume in single primary human neutrophils during activation by chemoattractant (Fig 1.1B-C). For stimulating cells in the FxM microfluidic chambers, we leveraged a UV-uncageable chemoattractant [5]. This enabled us to capture both the volume and motility response of cells before and after activation. Following chemoattractant-uncaging, the cells spread and transformed into a motile, amoeboid state with high persistence (Fig 1.1C). Simultaneously measuring the single cell volumes reveals a biphasic volume response (Fig 1.2A). Immediately following chemoattractant exposure, the cells lose ~5-8% of their cell volume (Fig 1.2A, inset), consistent with spreading-

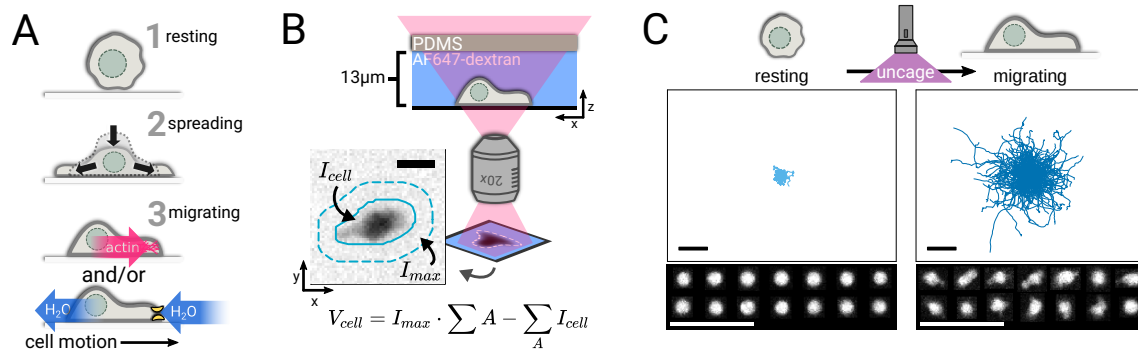


Figure 1.1: Fluorescence exclusion assay for measuring neutrophil volume during chemokinesis

(A) Schematic detailing the neutrophil activation process. Resting cells first spread and then begin migrating using cytoskeletal and/or osmotic forces. (B) Schematic detailing the Fluorescence Exclusion Microscopy (FxM) approach for measuring single cell volumes. This technique relies on cells displacing an extracellular dye in a shallow microfluidic chamber. The presence of a cell reduces the signal and the cell volume is equal to the difference between the measured signal over the cell's area and the expected signal if the cell was not there. The inset shows an example cell with the inner solid teal line indicating the cell footprint and the outer dashed line indicating the local background. The scale bar is 10 μ m. (C) Primary human neutrophil tracks over 15 minute time windows before (left) and after (right) the uncaging of the fMLP chemoattractant. Bottom panel has enlarged images of randomly selected example cells detailing neutrophil shape before and after activation. All scale bars are 50 μ m.

induced volume losses previously observed in other cells [50]. Preventing cell spreading by depolymerizing the actin cytoskeleton with Latrunculin B abrogates this initial volume loss in neutrophil-like differentiated HL-60 (dHL-60) cells (Fig 1.6F). Following this spreading-mediated initial volume loss, the cells swelled significantly, reaching a median volume 15% larger than their resting volumes 20 minutes post-stimulation. The chemoattractant-induced spreading can be seen by the increased cell footprint area post-stimulation (Fig 1.2B).

The volume of the median cell increases significantly from 2-20 minutes following chemoattractant stimulation. However, this masks more complex behavior at the single cell level.

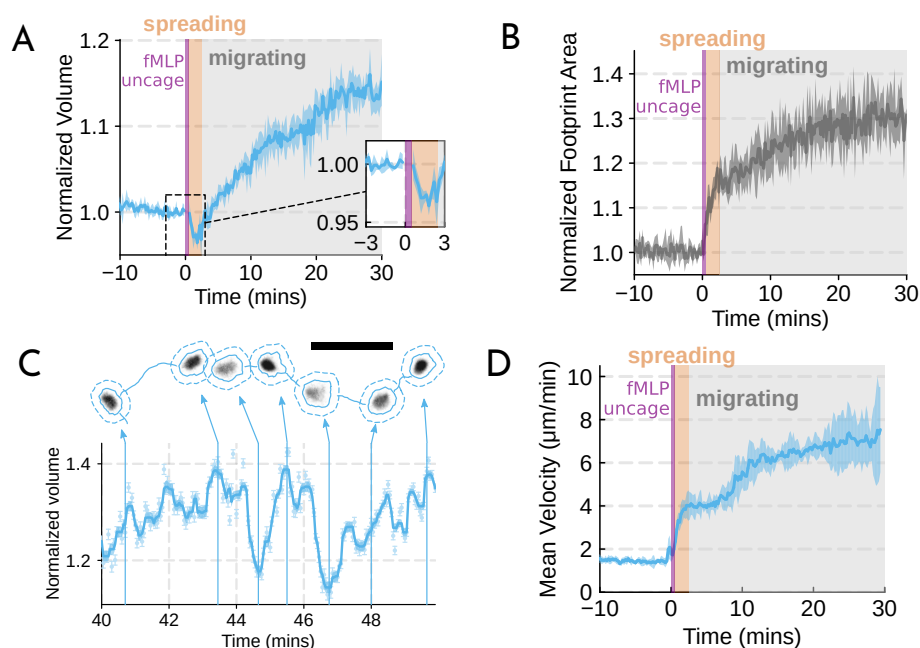


Figure 1.2: Chemoattractant stimulation elicits competing volume responses in primary human neutrophils

(A) Primary human neutrophil normalized volume responses following chemoattractant stimulation (Volunteer N = 4, Cells = 440 total). Inset details the volume loss due to spreading immediately after uncaging. Cells initially lose volume during the spreading phase following the chemoattractant stimulation and then significantly increase in volume. The line plotted is the average of the median cell response for each volunteer, and the shaded region is the 95% CI of the mean. For each volunteer, cell volumes are normalized to the volume in the two minute window prior to uncaging. (B) The normalized footprint area of primary human neutrophils responding to chemoattractant. The line is the average across biological replicates of median cell footprint area at each timepoint. Areas are normalized to the mean value in the two minute window prior to uncaging. The footprint area shows a monotonic increase in response to activation with cell spreading prior to initiation of movement. (C) Single representative cell trace imaged with high time resolution to highlight the cell motility-related volume fluctuations. Top section depicts the cell track with the FxM images overlaid at key time points that are linked with cyan arrows to the corresponding volumes in the bottom plot. Bottom half has faint cyan scatter points indicating the raw volume measurements with the thick cyan line depicting the rolling median volume. Scale bar is 50um. (D) Mean of the per-replicate median cell velocities computed at each time point. The shaded area is the standard deviation at each time point. Cell migration begins to increase in the early spreading phase following chemoattractant stimulation and then continues to increase over the next 20 minutes following stimulation.

Single-cell analyses reveal that even as the baseline volume has increased post-activation, individual cells exhibit large fluctuations in volume on the single-minute time scale as they move (Fig 1.2C). These appear correlated with the neutrophil motility cycle and require an intact actin polymerized cytoskeleton (Fig 1.6F). The increase in the volume set point (from 2 mins to 20-30 mins) is closely correlated with the increases in cell velocities over the same time frame (Fig 1.2D). To investigate whether there is a causal link between the chemoattractant-induced cell swelling and migration potentiation, we next sought to identify the molecular regulators of neutrophil swelling.

Genome-wide screen identifies regulators of chemoattractant-induced cell swelling

As an unbiased approach for identifying the regulators of chemoattractant-induced cell swelling, we turned to pooled genome-wide CRISPR/Cas9 screening [44]. Our approach relies on creating a population of cells with single gene knockouts and then enriching for the cells that fail to swell following stimulation. The quality of this enrichment is the most critical step for success of these screens [33]. A key challenge in adapting pooled CRISPR screening to this context was the lack of highly scalable approaches for accurately separating the cells based on their volumes directly. Although volume is difficult to use as a separation approach, cells can be easily separated by buoyant density (mass over volume), and buoyant density is related to volume over short timescales. Because neutrophil swelling in suspension

results from the uptake of water [17], stimulated neutrophils exhibit a corresponding decrease in buoyant density [37]. Buoyant density has been successfully used in other genetic screens, including the identification of secretion-defective mutants in yeast [34]. Finally, buoyant density is a particularly homogenous parameter at the population-level, with 100-fold less variation than either mass or volume across multiple different cell types [18].

To verify the chemoattractant-induced shifts in neutrophil buoyant density in our own hands, we deposited linear Percoll gradients (Fig 1.7A-B) in centrifuge tubes and carefully layered nutridoma-differentiated HL-60s (dHL-60s) onto the gradients in the absence or presence of the chemoattractant fMLP (Fig 1.3A). Stimulating dHL-60s with fMLP and using an optimized centrifugation protocol (Fig 1.7C) led to a robust, long-term decrease in buoyant density across millions of cells with a shift in population position clearly visible by eye (Fig 1.3B). The buoyant density change corresponded to a ~15% increase in cell volume (Fig 1.3C). This effect depends on chemoattractant-based cell stimulation, as knockout of the fMLP receptor FPR1 completely inhibits fMLP-induced swelling (Fig 1.3C, right).

To screen for the chemoattractant-induced regulators of cell volume, we transduced HL-60 cells with a commercial genome-wide CRISPR knockout library, differentiated them, and spun the cell population into Percoll density gradients with or without fMLP stimulation. We then fractionated the tubes and partitioned the samples into 3 different groups: low, medium, and high buoyant density (Fig 1.7D). We used next-generation sequencing to determine which CRISPR guides were over-represented in the high-density bin versus the other two bins, i.e. those that failed to swell and decrease in density following stimulation with fMLP

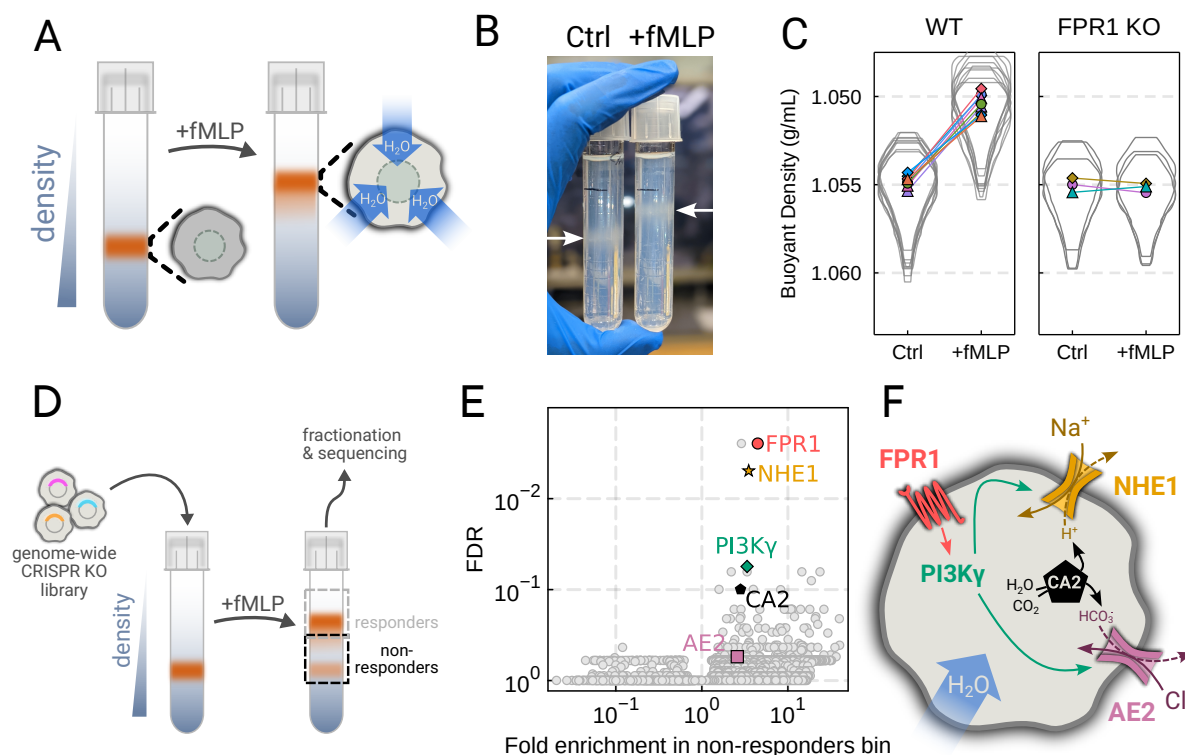


Figure 1.3: Genome-wide screen identifies regulators of chemoattractant-induced cell swelling

(A) Schematic detailing the buoyant density assay. The addition of fMLP causes cells to swell and decrease their density. As a result, the stimulated cells float higher in the Percoll density gradient. (B) Representative image of cell density shift following chemoattractant stimulation. Millions of cells appear as white fuzzy bands (indicated with the arrows). Cells in the right tube are stimulated with 20 nM chemoattractant (fMLP), causing them to swell and float higher in the gradient. (C) Violin plots quantifying the relative cell numbers as a function of density. Individual lines link replicate pairs. WT cells shift from 1.055g/mL to 1.050g/mL upon stimulation, while FPR1 KO cells do not shift following fMLP stimulation. (D) Schematic detailing the buoyant density-based genome-wide CRISPR knockout screen for identifying cells that are deficient at chemoattractant-induced cell swelling. (E) Volcano plot of the results of the chemoattractant-induced cell swelling screen. Genes that showed large inhibition of cell swelling and consistent behavior across their targeting guides appear in the upper right. The genes selected for further analysis are highlighted for a more complete list see Table 1.1. (F) Schematic outlining a potential pathway from chemoattractant stimulation to cell swelling.

(Fig 1.3D). To verify CRISPR knockout efficacy, we confirmed the systematic depletion of essential genes from the population (Fig 1.7E). Computing median log₂-fold enrichment of the guides targeting each gene in the dense bin and plotting this value against the false discovery rate reveals the regulators of chemoattractant-induced cell swelling (Fig 1.3E). The top right corner is occupied by genes that are over-represented in the dense, i.e. non-swelling, bin. The top hit was FPR1, the high affinity GPCR that specifically binds to fMLP to initiate the chemoattractant signaling cascade.

Our screen revealed a potential transduction cascade from the chemoattractant receptor to the final effectors of cell swelling, including the sodium-proton antiporter NHE1 (SLC9A1), the gamma subunit of phosphoinositide 3-kinase (PI3K), carbonic anhydrase II (CA2), and the chloride-bicarbonate exchanger 2 (AE2, i.e. SLC4A2) (Fig 1.3F). These hits suggest that the cell swelling cascade begins with fMLP binding to the chemoattractant receptor FPR1, which activates PI3K, which in turn activates NHE1 and AE2 which then work together to form the canonical regulatory volume increase (RVI) complex [20]. NHE1 and AE2 would, in this model, eject cytoplasmic protons and bicarbonate ions in exchange for extracellular sodium and chloride, respectively. CA2 catalyzes the production of protons and bicarbonate from CO₂ and water and directly binds the tail of NHE1 to enhance its activity [27, 28]. Thus, fMLP binding would lead to a net influx of sodium and chloride into the cell, mediating the influx of water and resulting in cell swelling.

Mechanistically separating chemoattractant versus motility-based volume changes

We next sought to individually validate our hits for chemoattractant-induced swelling. We created and verified single gene knockouts of the four components NHE1, AE2, PI3K, and CA2 using CRISPR/Cas9 in HL-60 cells. Using our buoyant density assay, we found that loss of either NHE1 or AE2 completely ablated the fMLP-induced volume increase in dHL-60s (Fig 1.4A). Our data indicate that both ion channels are needed for chemoattractant-induced swelling. Knockouts of PI3K and CA2 partially inhibited chemoattractant-induced swelling (Fig 1.8A).

Since dHL-60 cells exhibit significant basal migration even in the absence of chemoattractant stimulation, they are a non-ideal model for chemoattractant-stimulated migration compared to primary human neutrophils, which are completely quiescent and non-motile prior to stimulation. We next sought to replicate our knockout results through pharmacological inhibition of our CRISPR hits in human primary neutrophils. We used BIX (iNHE1), a potent and selective inhibitor of NHE1 [22], and Duvelisib (iPI3K), a potent PI3K/ inhibitor [53]. We compared chemoattractant-stimulated single cell volume responses in unperturbed, NHE1 inhibited (Fig 1.4B), or PI3K/ inhibited neutrophils (Fig 1.8B). Inhibition of either NHE1 or PI3K/ prevented chemoattractant-induced swelling in human primary neutrophils. At the single cell level, the NHE1 inhibited population brackets the initial cell volumes even 30 minutes post-stimulation, and this is consistent across days and replicates (Fig 1.4C). To

orthogonally verify the volume defect, we used a Coulter counter, an electronic particle sizing method, to measure the single cell volume responses following stimulation in suspension. These experiments confirmed that inhibition of NHE1 blocked cell swelling in suspension as well (Fig 1.8C). NHE1-inhibited cells maintained their ability to change shape and spread in response to chemoattractant, though they lagged behind control cells at later time points (Fig 1.4D). In contrast, PI3K/ inhibition blocked chemoattractant-induced shape change (Fig 1.8D).

Blocking NHE1 activity did not interfere with the spreading-induced volume loss of primary human neutrophils but it prevented the subsequent chemoattractant-induced volume gain. We next sought to determine whether the oscillatory volume fluctuations associated with the motility-cycle were affected by NHE1 inhibition. Performing high temporal resolution imaging of single cells at later time points (30-50 minutes) following uncaging revealed that the iNHE1 cells exhibit similar motility-coupled volume changes but at vastly different baselines (Fig 1.4E). So despite the motility-cycle-associated volume fluctuations being similar (Fig 1.8E), the baselines are approximately 20% decreased in NHE1 inhibited versus unperturbed cells following chemoattractant stimulation.

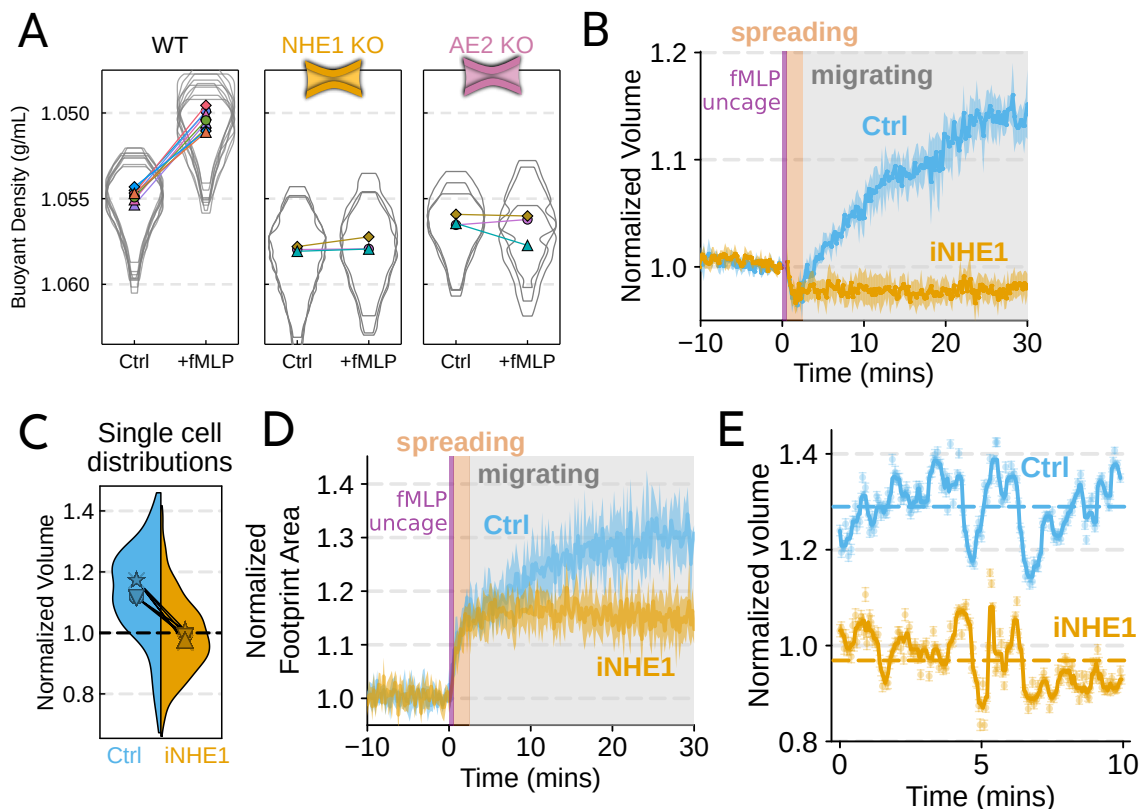


Figure 1.4: Mechanistically separating chemoattractant versus motility-based volume changes

(A) Knockout of NHE1 or AE2 is sufficient to completely inhibit the chemoattractant-induced swelling in neutrophil-like differentiated HL-60 cells (B) NHE1 inhibition in human primary neutrophils blocks fMLP-induced swelling but does not inhibit the spreading-induced volume loss. (Ctrl: Volunteer N = 4, iNHE1: Volunteer N = 6). (C) The distributions of single cell volumes 30 minutes post-chemoattractant stimulation demonstrates that the NHE1 inhibited neutrophils remain close to the pre-stimulation volumes, i.e. 1.0 on the ordinate (D) NHE1 inhibited neutrophils have similar increases in their footprint area to control cells when they spread and begin moving following fMLP stimulation, but lag control cells at later time points (E) High temporal resolution imaging of the motility-induced volume fluctuations starting at 30 minutes post-stimulation demonstrate that both control and NHE1-inhibited neutrophils show similar short-term volume fluctuations around significantly different baselines (dashed lines).

The chemoattractant-driven volume gain is necessary and sufficient for rapid migration

We next sought to leverage our identified volume regulators to probe the relation between cell swelling and motility. Turning again to the FxM assay, we activated primary human neutrophils by uncaging fMLP and measured the average cell velocity over the population (Fig 1.5A). In the first 10 minutes following uncaging, both WT and NHE1-inhibited cells both exhibited a similar potentiation of migration. However, after 10 minutes the unperturbed neutrophils continued increasing in speed, while the iNHE1 cells plateaued. The WT speed potentiation is closely correlated with the kinetics of swelling. To visualize the volume-velocity relationship, we plotted the average volume versus average speed of single WT cells in the first 10 minutes following uncaging versus 20-30 minutes post-uncaging (Fig 1.5B). In the early time points following chemoattractant stimulation, control cells operate in a low-volume, low-velocity regime. At later time points following stimulation, control cells operate in a higher-volume high-velocity state. The iNHE1 cells persist in the low-volume, low-velocity state even 20-30 minutes post stimulation (Fig 1.5C). To test whether other aspects of chemokinesis are affected in the iNHE1 cells, we also computed the angular persistence of single cells over 10 micron distance windows and found no difference in between WT and iNHE1 cells (Fig 1.9A). This is in contrast to the PI3K⁻-inhibited cells, which failed to increase their velocity following chemoattractant uncaging (Fig 1.9B).

NHE1-inhibited cells are defective in both chemoattractant-induced swelling and rapid

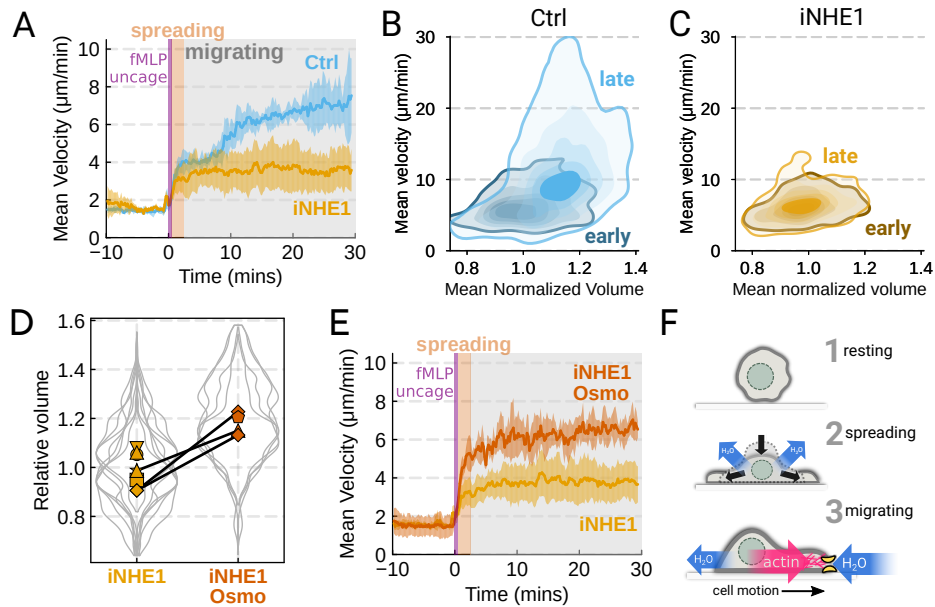


Figure 1.5: The chemoattractant-driven volume gain is necessary and sufficient for rapid cell migration following stimulation

(A) Comparison of control (cyan) or NHE1-inhibited (gold) primary human neutrophil migration following chemoattractant stimulation. Mean of the per-replicate median cell velocities is shown, with the shaded area indicating standard deviation at each time point. (Ctrl: Volunteer N = 4, iNHE1: Volunteer N = 6). (B) Contour plots of the average velocity versus average normalized volume for single unperturbed neutrophils for the initial 10 minute window following stimulation (early) and from 20-30 minutes following stimulation (late) (C) Contour plots of the average velocity versus average normalized volume for single NHE1-inhibited neutrophils for the initial 10 minute window following stimulation (early) and from 20-30 minutes following stimulation (late) (D) Dilution of imaging media with 20% water led to a ~15% increase in the median cell volumes of iNHE1 cells (iNHE1 Osmo; red) versus iNHE1 cells in normal media (gold). Volumes are normalized relative to the median iNHE1 cell volume. This is similar to the magnitude of chemoattractant-induced swelling in control cells. The black lines connect conditions where both conditions were measured for the same volunteer. (iNHE1 Osmo: Volunteer N = 3, 4 total replicates; iNHE1: Volunteer N = 6) (E) Exogenous cell swelling via hypoosmotic shock is sufficient to rescue the migration defect in NHE1-inhibited neutrophils. Mean of the pre-replicate median cell velocities computed at each time point for NHE1 inhibited cells (yellow) versus mildly hypoosmotically swollen NHE1 inhibited cells (red). Shaded area is the standard deviation at each time point. (iNHE1 Osmo: Volunteer N = 3, 4 total replicates; iNHE1: Volunteer N = 6). (F) Summary schematic. Cell swelling collaborates with actin polymerization to potentiate chemoattractant-induced cell migration.

migration. To determine if the lack of cell swelling is the basis of their migration defect, we sought to rescue cell swelling for iNHE1 cells through a mild hypoosmotic shock. Diluting the media 20% (v/v) with water led to a ~15% increase in volume of the iNHE1 cells, approximating the magnitude of swelling elicited by fMLP in control cells (Fig 1.5D). Uncaging fMLP initiated chemokinesis for both iNHE1 and iNHE1-Osmo cells, but the hypoosmotically shocked cells continued accelerating for longer and reached higher sustained speeds (Fig 1.5E). Intriguingly, the hypoosmotically shocked cells are precocious in their rapid motility. This might be expected, since these cells are pre-swollen prior to stimulation, whereas control cells take longer to reach the high-volume high-velocity state following chemoattractant stimulation. Our data suggest that the water influx following chemoattractant stimulation plays an important role in the potentiation of neutrophil migration (Fig 1.5F).

1.3 Discussion

Neutrophils are remarkable for the rapid migration that is key to their innate immune function [25]. Here we show that human primary neutrophils actively increase their cell volumes when stimulated with chemoattractant, and this correlates with their rapid movement (Fig 1.2). We then perform an unbiased genome-wide screen to identify the molecular components of chemoattractant-induced cell swelling (Fig 1.3D-F). While one of the hits, NHE1, has been investigated in previous studies [8, 13, 39, 54], our work systematically identifies the dominant players in a larger network that contribute to the swelling response. Buoyant

density screening was used with great success by Schekman and colleagues to elucidate the secretory pathway in yeast [34, 35]. Here, we use the sensitivity of this assay combined with the power of modern forward genetics to uncover the mechanistic basis of how cells actively manipulate their volume to enhance migration.

Our work implicates both NHE1 and AE2 in cell swelling, as knockout of either completely ablates chemoattractant-induced swelling in dHL-60 cells (Fig 1.4A). PI3K/ inhibition was sufficient to prevent swelling in primary human neutrophils while also blocking chemokinesis (Fig 1.8B,1.9B). This agrees with earlier work demonstrating an essential role for PI3K activity in neutrophil chemokinesis [12]. Finally, knockout of CA2 also reduced swelling in dHL-60s (Fig 1.8A), supporting the previously reported role of CA2 in enhancing the activity of NHE1 [27, 49]. We then confirmed our dHL-60 results via pharmacological inhibition of NHE1 in human primary neutrophils and verified the necessity of NHE1 in the chemoattractant-induced swelling response (Fig 1.4). NHE1-inhibited cells showed a defect in both motility and chemoattractant-induced swelling (Fig 1.5A-C). This agrees with previous work mostly in slow-moving immortalized cell lines where NHE1 is critical for optimal motility [8, 24, 47, 54]. In contrast, previous work in chemotaxing primary human neutrophils suggested only a housekeeping role for NHE1 in preventing the acidification of the cytoplasm [19]. Consistent with previous results, we observe only minor defects for NHE1-inhibition in the first 10 minutes following chemoattractant stimulation. At longer time points, NHE1-inhibited cells fail to continue their migration acceleration compared to uninhibited cells. This lack of migration potentiation in NHE-1 inhibited cells can be ex-

plained by their defective cell swelling, as exogenous swelling via hypoosmotic shock rescues the velocity defect (Fig 1.5D-E).

How might swelling contribute to rapid neutrophil migration? Given that neutrophils are approximately 65% water (Fig 1.7F), the 15% increase in cell volume corresponds to almost a ~25% increase in the water content of the cell after 20 minutes. This change could affect global biophysical parameters such as a decrease in cytoplasmic viscosity or an increase in the diffusion of biochemical or cytoskeletal regulators of movement. Alternatively or in addition, local water influx could collaborate with the actin polymerization machinery in facilitating the extension of the plasma membrane [14, 32]. The regulatory volume components identified here are ubiquitously expressed, so it is possible that they also facilitate chemoattractant-induced migration in other contexts. NHE1-dependent swelling has been observed in dendritic cells responding to LPS [41], and NHE1 inhibition slows microglial chemotaxis [45]. NHE1s role in migration and metastasis is well-established [47, 54], and several other constituents of our chemoattractant-induced cell swelling program have been implicated in cell migration responses as well. AE2 plays a role in murine osteoclast spreading and migration [6]. Similarly, carbonic anhydrases have been implicated in facilitating migration [48], and PI3K isoforms have a well-appreciated role in migration [9, 12]. Systematic investigation of this chemoattractant-induced cell swelling network could reveal a general role for water influx in potentiating cell migration.

Table 1.1: Chemoattractant-induced swelling genome-wide CRISPR KO screen hits

Rankings determined using MAGeCK [26]. Fold change is the median fold enrichment in the dense bin versus the other two bins of the functional guides. FDR is the false discovery rate of each gene given the distribution of negative control guides in the library. See Methods section for details.

Ranking	HUGO ID	Fold Change	FDR	# Good sgRNAs	Common Name
1	FPR1	4.4617	0.00248	3	FPR1
2	STAT3	2.8815	0.00248	4	
3	SLC9A1	3.5013	0.00495	4	NHE1
4	PIK3CG	3.3557	0.05569	4	PI3K
5	MARS2	23.6178	0.06374	3	
6	NUP35	14.5253	0.06374	3	
7	SKA1	3.3554	0.06374	4	
8	CA2	2.8157	0.09942	4	CA2
9	CANX	3.966	0.09942	4	
10	COPS3	8.2426	0.10015	4	
11	RPS2	18.7498	0.07976	3	
12	TPR	9.6024	0.16455	4	
13	RFT1	26.2401	0.16455	2	
14	SETD1A	11.1409	0.16455	2	
15	TP53TG3C	11.2083	0.16455	3	
16	UHRF1	4.7194	0.16455	3	
17	THG1L	10.4411	0.16455	3	
18	MRPL20	10.8506	0.16455	4	
19	UTP11L	9.0882	0.16455	3	
20	TPI1	17.976	0.16455	3	
21	CT47A6	2.8505	0.16455	3	
22	ESCO2	11.9249	0.1982	4	
23	GRXCR2	2.8457	0.1982	4	
24	PARP12	21.181	0.1982	2	
25	NR1H2	39.6651	0.20894	2	
100	SLC4A2	2.582	0.54636	2	AE2

Table 1.2: Volunteer Demographic Information

Demographic information collected for the volunteer donors according to the Institutional Review Board-approved study protocol at the University of California - San Francisco (Study #21-35147)

Volunteer	Age	Sex
4	27	M
5	30	M
6	37	F
8	31	M
14	24	M
17	29	F
18	28	M
19	30	M

Table 1.3: Guides used to make single gene knockouts in HL-60s

The two highest performing guides from the genome-wide screen were chosen to make single gene knockouts in the HL-60 cell line. See Methods for details.

HUGO gene name	Takara sgRNA ID	Guide Sequence (5' -> 3')	Internal ID
FPR1	sgFPR1_2	CTACAGTACCTGGTAAAACG	11
FPR1	sgFPR1_3	CTGACAGCAACGATGGACAT	12
SLC9A1	sgSLC9A1_2	TTTGCCAACTACGAACACGT	13
SLC9A1	sgSLC9A1_4	TGAGGAACAGGTCACACATG	15
PIK3CG	sgPIK3CG_1	ACTTAACCCTCTCACAGCAG	16
PIK3CG	sgPIK3CG_3	GAGAATACGTCCTCCACATG	18
CA2	sgCA2_2	TATGAGTGTCGATGTCAACA	19
CA2	sgCA2_4	TCACTGGAACACCAAATATG	20
SLC4A2	sgSLC4A2_2	ACCTGCCCCACATACCCACA	21
SLC4A2	sgSLC4A2_3	GAAGACGCAGGACCTGATAG	22
NegCtrl	Neg_Control_Human_0067	GGTAGGACCTCACGGCGCGC	23
NegCtrl	Neg_Control_Human_0084	GCTGTTCGTGTGGAGGCTATG	24

1.4 Materials and methods

Medias and Inhibitors

For all imaging experiments, imaging media was made with Phenol Red-free Leibovitz's L-15 media (Gibco #21083027) supplemented with 10% (v/v) heat-inactivated fetal bovine serum

(Gibco) and filtered with a 0.22 μm Steriflip filter (MilliporeSigma #SCGP00525). Imaging media was always prepared fresh on the same day of imaging. For FxM coating, 0.2% endotoxin and fatty acid-free Bovine Serum Albumin (BSA) (Sigma #A8806) was dissolved in L15 via pulse centrifugation. The mix was then filtered with a Steriflip filter before further use. For all density experiments, divalent-free mHBSS media was prepared as in Houk et al [21]. In short, 150 mM NaCl, 4 mM KCl, 10 mg/mL glucose and 20 mM HEPES were dissolved in Milli-Q (Millipore) water and the pH adjusted to 7.2 with 1M NaOH. The osmolarity was verified to be 315 mOsm/kg on a micro-osmometer (Fiske Model 210). Culturing media (R10) was made from RPMI 1640 media (Gibco #11875093) supplemented with 25mM HEPES and L-glutamine supplemented with 10% (v/v) heat inactivated fetal bovine serum (Gibco). The NHE1 inhibitor, BIX (Tocris #5512), was dissolved in dry DMSO to a final concentration of 25 mM and stored at -20 in single use aliquots that were diluted in imaging media the day of the experiment. All iNHE1 experiments used BIX at a 5 μM final concentration. Similarly, Latrunculin-B (Sigma #428020) was stored at 10 mM in DMSO and used at 1 μM final. For PI3K/ inhibition, Duvelisib (MedChemExpress #HY-17044) was stored at 10 mM in DMSO and used at a final concentration of 1 μM .

Human primary neutrophil isolation and drug treatment

All blood specimens from patients were obtained with informed consent according to the institutional review board-approved study protocol at the University of California - San

Francisco (Study #21-35147), see Table 1.2 for demographic information. Fresh samples of peripheral blood from healthy adult volunteers were collected via a 23-gauge butterfly needle collection set (BD #23-021-022) into 10 ml Vacutainer EDTA tubes (BD #366643). Blood was kept on a shaker at minimum setting and utilized within 2 hours of the draw. Neutrophils were isolated using the EasySep Direct Human Neutrophil Isolation Kit (STEMCELL Tech #19666) with the BigEasy magnet (STEMCELL Tech #18001) according to the manufacturers protocol.

Isolated neutrophils were spun down at 200g for 5 min and resuspended in a dye media consisting of imaging media containing 5ug/ml Hoechst 3334 (Invitrogen #H3570) and 0.25 uM Calcein Red-Orange AM (Invitrogen #C34851). This cell suspension was incubated at room temperature in the dark for 15 min, and then the cells were spun down at 200g for 5 min. The dye medium was aspirated and replaced with R10 to achieve a final cell density at or below 1×10^6 cells/mL. Purified neutrophils were then kept in polystyrene T25 flasks (Corning) at 37 in a 5% CO₂ environment until imaging. Cells were used ~5-8 hours post-isolation.

Cell culture

Short tandem repeat authenticated HL-60 cells [42] were maintained in R10 media at 5% CO₂ and 37 and at a concentration of 0.2-1 million/mL by passaging every 2-3 days. 5 days prior to experiments, HL-60s were differentiated into a neutrophil-like state by taking an aliquot

of cells in their culturing medium and supplementing with an equal volume of Nutridoma-CS (Roche #11363743001) and DMSO diluted in RPMI such that that the final concentrations were 0.2 million/mL HL-60 cells, 2% (v/v) Nutridoma-CS, 1.3% (v/v) DMSO, 5% (v/v) FBS in RPMI. After 5 days at 37/5% CO₂, we observed robust expression of terminal differentiation markers like FPR1 as reported previously [38].

Lenti-X HEK-293Ts (Takara) were used for lentivirus production and maintained at below 80% confluency in DMEM supplemented with 10% (v/v) heat-inactivated fetal bovine serum. These cells were also maintained at 5% CO₂ and 37. All cell lines were routinely monitored for mycoplasma contamination using standard mycoplasma monitoring kits (Lonza).

FxM single cell volume measurements

FxM microfluidic chips were prepared as previously described [4, 55] using a custom mold generously provided by the Piel lab. Briefly, 10:1 (w/w) PDMS elastomer base and crosslinker (Momentive #RTV615-1P) were thoroughly mixed, poured into the FxM mold, and degassed under a vacuum for one hour. The PDMS was then baked at 80°C for 2 hours and removed from the mold. The day prior to experiments, the molded PDMS was cut with a scalpel to form 3 lane chips” and the inlet and outlet holes were created using a 0.5mm punch. The chips and 35mm glass-bottomed dishes (Willco Wells #HBST-3522) were then plasma cleaned for 30 s, and chips were gently pressed down onto the glass to form a watertight seal. A good seal was verified visually by the refractive index change upon glass/PDMS contact.

The chips were then baked at 80°C for 10 minutes to ensure thorough bonding. The chips were then quickly coated with 100 ug/mL human fibronectin (Sigma #SLCL0793) diluted in PBS and injected using a pipette tip. Coating was allowed to proceed for 30 minutes at RT before the chamber was flushed with imaging media. The chips were then submerged in PBS and allowed to incubate with L15 + 0.2% BSA overnight at 4°C.

On the day of the experiment, pre-prepared microfluidic chips were allowed to warm up at RT. Human primary neutrophils were gently pipetted up and down to resuspend if they had settled and spun down at 200xg for 4 minutes. The cell pellet was very slowly resuspended in imaging media to achieve a cellular concentration of 60 million per mL. The cells were allowed to equilibrate for 30 minutes at RT. The lanes of the chip were flushed with the corresponding final media. The cells were gently mixed with a 2x solution such that the final concentrations were 0.5mg/mL Alexa Fluor 647-tagged 10,000 MW dextran (Invitrogen #D22914), 200nM caged fMLP (NEP), and 30 million per mL cells in imaging media. This mixture was then slowly pulled into the chamber using a partially depressed pipette tip to minimize the shear forces on the cells, as these are known to affect neutrophil response to fMLP [31]. Once loading was complete, the entire chamber was submerged in imaging media to stop all flows and allowed to warm up to 37. Experiments were started promptly 20 minutes post-submersion.

Suspension cell volume measurements

Suspension cell volume measurements were performed as in Graziano et al [16]. Briefly, human primary neutrophils were spun out of culture media at 200xg for 4 minutes and gently resuspended in mHBSS. They were then diluted to 20,000 cells/mL in warm 15mL of mHBSS in Accuvettes (Beckman-Coulter). The cells were incubated at 37°C for 5 minutes, and then either a DMSO blank or the indicated amount of drug was added to the correct final concentration. The cells were again incubated for 5 minutes at 37°C. They were then quickly transported to the Multisizer Z2 instrument (Beckman-Coulter) at RT. Three time points were taken to set a baseline, and then fMLP (Sigma) was added to a final concentration of 20 nM, and the Accuvette was inverted to mix. Then 0.5 mL samples were taken continuously every minute using a 100 um diameter aperture with a current of 0.707 mA, a gain of 64, a pre-amp gain of 179.20, a calibration factor (Kd) of 59.41 and a resolution of 256 bits. 5000-10,000 cells were sampled per time point and the medians of the population was extracted using our software available at <https://github.com/tlnagy/Coulter.jl>

Buoyant Density Measurements

Buoyant density measurements were done by pre-pouring gradients, layering dHL-60s on top, centrifuging, fractionating, and then imaging to count cells. First, solutions were made with either 32.6% or 57% (v/v) Percoll (Sigma) with 10% (v/v) 10x divalent-free mHBSS and diluted with ultrapure water, making a low density solution (LDS) and high density solution

(HDS), respectively. The refractive index of both solutions was determined with a MA871 refractometer (Milwaukee Instruments) as 1.3419 and 1.3467, respectively. Given that the density is linearly related to the refractive index (Fig S2A) the solutions have densities of 1.045 g/mL and 1.074 g/mL, respectively. For the chemoattractant-condition, 20 nM fMLP (Sigma) was added. A linear gradient mixer was attached to an Auto Densi-Flow (Labconco) gradient fractionator and used to dispense gradients into 14 mL round bottom tubes (Falcon #352041).

For each gradient, approximately 5 million dHL-60s were spun down at 200xg for 4 minutes and resuspended in 1mL of 1x mHBSS. The cells were then labeled with 0.5 μ M Calcein-AM (Invitrogen) for 5 minutes then spun down and resuspended in LDS. For mixed populations, the two cell types were spun down and labeled separately with either Calcein-AM or Calcein Red-Orange-AM and then mixed together. The cells were layered gently on top of the gradient and spun at 250xg for 1 hour. Neutrophils display homotypic aggregation when activated during centrifugation [46] so we used a divalent-free media and very long centrifugation times optimized for separation at low centrifugation speeds (Fig 1.7C).

After centrifugation, the cells were fractionated into a 96-well using the Auto Densi-Flow in remove modality and a homemade fractionator. 6-7 wells were taken, and their refractive index was measured using the refractometer to align the gradients and verify linearity (Fig 1.7B). A 2x volume of blank media was added to each well to reduce the density, and then the plates were spun in the centrifuge at 250xg to assist the settling of the cells on the glass. The plates were then imaged using confocal microscopy to determine the number of cells in

each well. For mixed population experiments, dual color imaging was done to determine the cell count of each sample.

CRISPR Genome Wide Screen on Buoyant Density

Lenti-X 293Ts (Takara) were transfected with the Guide-it library (Takara) according to the manufacturers instructions and concentrated $\sim 100\times$ using the Lenti-X concentrator kit (Takara) and stored at -80°C until needed. Human codon-optimized *S. pyogenes* Cas9-tagBFP expressing HL-60 cells [16] were transduced by spinoculating the cells on Retronectin-coated (Takara) non-TC treated 6-well plates (Falcon #351146). Briefly, each well was coated with 20ug/mL Retronectin stock solution diluted in DPBS for 2 hours and then blocked with 2% BSA (w/v) in PBS for 30 minutes and washed with PBS. 2mL of 1 million/mL Cas9-BFP HL-60s were added to each well of 4 plates (48 million cells total) and 30uL of concentrated Guide-it library lentivirus was added to each well. Using Lenti GoStix (Takara), we estimated that this corresponds to 8×10^6 IFUs per well. The plates were spun at 1000xg for 30 mins, and then 1mL of R10 was added gently. This was followed by another dilution with 2 mL of the same media after 24 hours. 48 hours post spinoculation, the cells were spun down at 200xg and resuspended in R10. The cells were then sorted for mCherry-positive cells (cutoff set at 99.9th percentile of the untransduced cell populations mCherry signal) using a FACSAria 3 cell sorter (BD). We observed 4% of cells with a mCherry positive signal, equivalent to a MOI of 0.04. This gives a minimum coverage of 6-24x of the library at

transduction; post-sequencing Monte Carlo simulations suggest a minimum coverage of 12x. After sorting, the cells were selected using 175 ug/mL hygromycin and kept in log-phase growth with regular supplementation with fresh media for 7 days, after which ~95% of the population were mCherry positive.

5 days prior to screening day, the cells were differentiated into neutrophil-like cells as described in the Cell Culture section. The buoyant density assay was performed as described in the Buoyant Density Measurements section with 6 million cells per tube split across 6 tubes, corresponding to 36 million cells or ~450x coverage of the library. The cells were layered on top of the gradients containing 20 nM fMLP with or without 1 uM Latrunculin-B, and then each tube was fractionated into 48 wells, which were combined into 3 separate bins such that they each contained approximately one third of the population (Fig S2B). The bins from each tube belonging to the same sample were combined, and then the cells were spun down, and the pellets were flash frozen to store for further processing. The genomic DNA was extracted using the QIAamp gDNA kit (Qiagen) according to the manufacturers instructions. The guides were then PCR amplified for 26 cycles using the Ex Taq polymerase (Takara) protocol with the P5 forward primer mix (Takara) and a unique reverse P7 primer for each condition. The specificity and quality of amplification for each sample was validated using a TapeStation 4200 (Agilent), and the precise DNA concentration was determined using a Qubit fluorometer (Invitrogen) according to manufacturers instructions. The amplified DNA was then pooled to a 10 nM final concentration followed by a 5% PhiX (Illumina) spike and sequenced in a PE100 run on a HiSeq 4000 sequencer (Illumina) at the UCSF sequencing

core.

To verify that we can detect the functioning of Cas9, we assayed for the depletion of guides targeting previously published essential genes [11, 51]. We used MAGeCK [26] to compute the log fold change between the known frequencies of the guides in the library (Takara) and the actual observed frequencies of the guides (computed by pooling all bins together). The cumulative distribution of the essential gene ranks were compared to a randomly shuffling of those same genes to demonstrate that the essential genes were highly depleted from the population, as expected (Fig 1.7E).

Similarly, to determine which genes were involved in the chemoattractant-induced density change, we used MAGeCK to compute the false discovery rate and log fold change between the first and second bins vs the third bin (Fig 1.7D). The third bin was the most dense bin, so genes over-represented in this bin versus the other two were likely interfering with the swelling process. We pooled the samples with and without 1 μ M Latrunculin-B together to improve our sensitivity as the swelling is not dependent on a polymerized cytoskeleton (Fig 1.6F). The combined fold change for each gene was then computed by taking the MAGeCK alphamedian log fold change (either positive or negative) that was most divergent. Using this fold change and the false discovery rate, we identified the genes that are most likely involved with the chemoattractant-induced swelling (Fig 1.3E, Table 1.1).

Single gene knockout line generation with CRISPR/Cas9

Single gene knockouts were generated and validated using wildtype HL-60s expressing human codon-optimized *S. pyogenes* Cas9-tagBFP cells as the base line as previously described [16]. The two best performing guides from the genome-wide screen (Table 1.3) were selected and synthesized (IDT) and then cloned into the pLVXS-sgRNA-mCherry-hyg Vector (Takara) following the manufacturers instructions. Lentivirus was then produced as previously described [16]. Briefly, LX-293T cells (Takara) were seeded into 6-well plates and grown till 80% confluence was reached. 1.5 g of the guide vector (from above) was mixed with 0.167 g vesicular stomatitis virus-G vector and 1.2 g cytomegalovirus 8.91 vector. This mixture was incubated with the TransIT-293 Transfection Reagent (Mirus Bio) and used to transfect the 293T cells following the manufacturers instructions. The cells were grown for 72 hours post-transfection and the virus was concentrated ~40-fold from the supernatant using the Lenti-X concentrator kit (Takara) per the manufacturers protocol. Concentrated virus stocks were stored at -80°C until needed. For transduction, virus stocks were thawed and added to 300,000 cells in R10 in the presence of polybrene (8ug/mL) and incubated for 24 hours. Afterwards, the cells were washed twice with R10 to remove any remaining viral particles and sorted for mCherry-positivity on a FACSAria 3 cell sorter (BD). The heterogeneous population was then assayed for successful editing by sequencing the genomic DNA flanking the Cas9 cut site. Clonal populations were then isolated by seeding dual BFP and mCherry-positive cells into a 96-well plate such that only one cell was deposited in each well

using a FACS Aria Fusion (BD). The cells were then allowed to grow up and clonality was verified by genomic DNA sequencing of the cut site as previously described [15].

Microscopy Hardware

FxM and buoyant density experiments were performed on an inverted Eclipse TI microscope (Nikon) with a Borealis beam conditioning unit (Andor), and light was collected on an air-cooled iXon 888 Ultra EM-CCD (Andor). A 20x Plan Apochromat NA 0.75 objective (Nikon) was used for FxM, and a 10x Plan Apochromat (Nikon) was used for density experiments. Light sources include a Stradus Versalace 405, 488, 561, 647-nm laser line system (Vortran Laser Technologies) and a Sutter Lambda LS xenon-arc lamp used for FxM. Microscopy hardware was controlled with a TriggerScope 4 (Advanced Research Consulting) via MicroManager [10].

UV light for uncaging was delivered via a 365nm Lambda FLED (Sutter) launched into a Lambda OBC and delivered via the condenser with all mobile optical elements removed and all apertures wide open. Before every experiment, the wattage was measured using a light meter (Thor Labs). The LED was controlled via a custom MicroManager script.

Data Analysis

FxM images were analyzed using a custom pipeline (Fig S1A) implemented in the Julia language [2] available at <https://github.com/tlnagy/FluorescenceExclusion.jl>. Briefly,

the raw images were denoised with a patch-based algorithm [3] and then the edges were enhanced using a Scharr kernel. The magnitude of the edge values is log normally distributed, and we empirically determined that calling the edge of the cell at 1 standard deviation above the mean gave low noise and the maximum signal (Fig 1.6C). Flood-filling the areas encapsulated by these edges gave a binary mask of the foreground, i.e. space occupied by the cells.

Independently, instance segmentation was performed using a custom Cellpose model trained using the human-in-the-loop feature [36] on the raw nuclear and cytoplasmic channels. Trackpy was used to link the Cellpose segmented instances together in time [1] and these were then used to nucleate a watershed algorithm on the binary mask of the foreground and separate the foreground into the individual tracked cells. Next, the raw image was flatfield corrected by fitting a multiquadratic function at sinusoidally placed locations (avoiding the locations of cells or pillars) in the raw image which gave the densest sampling at the edges. Given that the chambers have flat ceilings supported by pillars [55], the background signal can be used to compute the per-time point flatfield. After subtracting the darkfield image from both the raw FxM signal and the interpolant, the raw signal was divided by the interpolant giving extremely uniform homogeneous signal across the FOV.

Next, the local background was computed for each cell which we defined as the region 2 to 10 pixels away (1.3 to 6.5 microns) from the cell borders while avoiding other cells. The median of this local background was used to compute the counterfactual of what the signal would have been if the cell was not there by multiplying by the pixel area of the cell A (Fig

1.1B, inset). The measured signal over the area of the cell was then subtracted from that value to give the volume excluded by the cell according to equation 2 from [4]:

$$V_{cell} = \sum_{x,y \in A} \frac{I_{max} - I_{cell}(x,y)}{\alpha} \quad (1.1)$$

where I_{max} is the median signal of the locality, i.e. the maximum signal if the cell was not there. A is the cell footprint area and I_{cell} is the signal at each point $x, y \in A$. To convert this to absolute volume measurements we divide by α which is the fluorescence as a function of object height:

$$\alpha = (I_{max} - I_{min})/h_{chamber} \quad (1.2)$$

Where the minimum signal I_{min} is the signal at the pillars that support the chamber's roof and $h_{chamber}$ is the height of the chamber in microns. As discussed in [4], while the per-pixel heights might not be accurate due light scatter, segmenting a slightly larger area than the cell footprint (1.6C) captures any scattered signal and yields accurate whole cell volumes.

For velocity measurements, cell tracks were analyzed using the following equation to compute the velocity at frame i over a window τ given the x and y coordinates in microns and time t in seconds:

$$\nu_i = \frac{\sqrt{(x_{i+\tau} - x_{i-\tau})^2 + (y_{i+\tau} - y_{i-\tau})^2}}{t_{i+\tau} - t_{i-\tau}} \quad (1.3)$$

For all plots in this paper a τ of 3 corresponding to approximately a one minute window was used, but similar results were obtained at other values of τ .

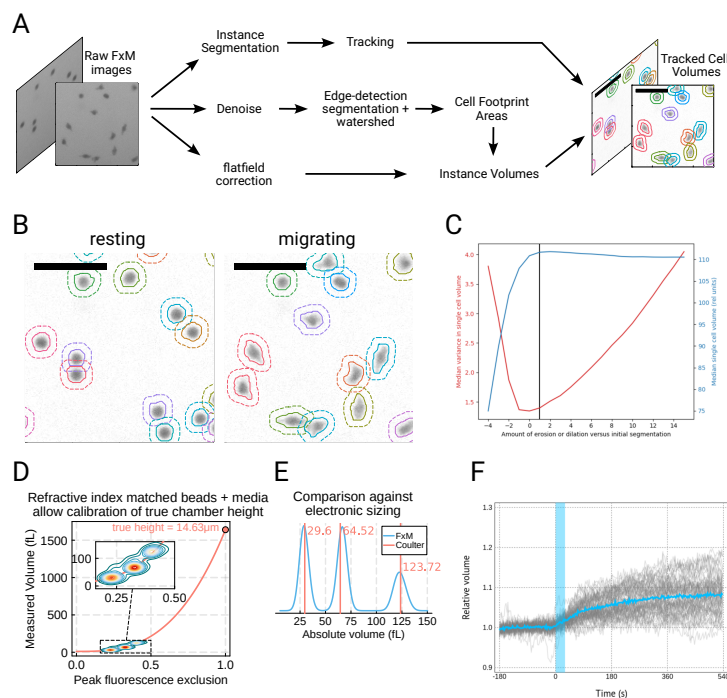


Figure 1.6: Validation of the Fluorescence eXclusion Microscopy pipeline

(A) Overview of the modified FxM pipeline used in this work. Raw FxM images are segmented into seeds, which are then tracked. To identify cell boundaries, we use a custom algorithm that involves denoising the raw FxM followed by edge detection and watershedding that was nucleated at the seeds. Finally, to extract the volumes we apply minimal processing with a custom flatfield correction algorithm followed by extraction using the previously-determined cell boundaries. (B) Examples of resting (left) and migrating (right) cells segmented and tracked using the pipeline above (1.6A). (C) Quantifying the signal-to-noise tradeoff with the edge detection. Overly conservative or overly liberal segmentation leads to non-optimal volume measurement. The chosen cutoff (black line) balances the noise (red) and measured volume (blue). This was computed on unstimulated cells. (D) Injecting beads into the FxM chambers in refractive-index media to minimize distortions allows for true calibration of chamber height. The contour plot of the per-bead max signal depth (i.e. height of the beads from FxM) vs the measured volume using FxM is well fit by the spherical volume formula (salmon line). The intersection of this line with 1.0 on the abscissa is equivalent to a sphere that completely fills the chambers and indicates the true height of the chamber. (E) Comparing calibrated FxM volumes of the beads (cyan) against the gold standard Coulter counter (salmon) shows good agreement. (F) dHL-60 cells treated with 1 μ M Latruculin-B swell in response to chemoattractant stimulation but lack cell spreading and spreading-related volume loss.

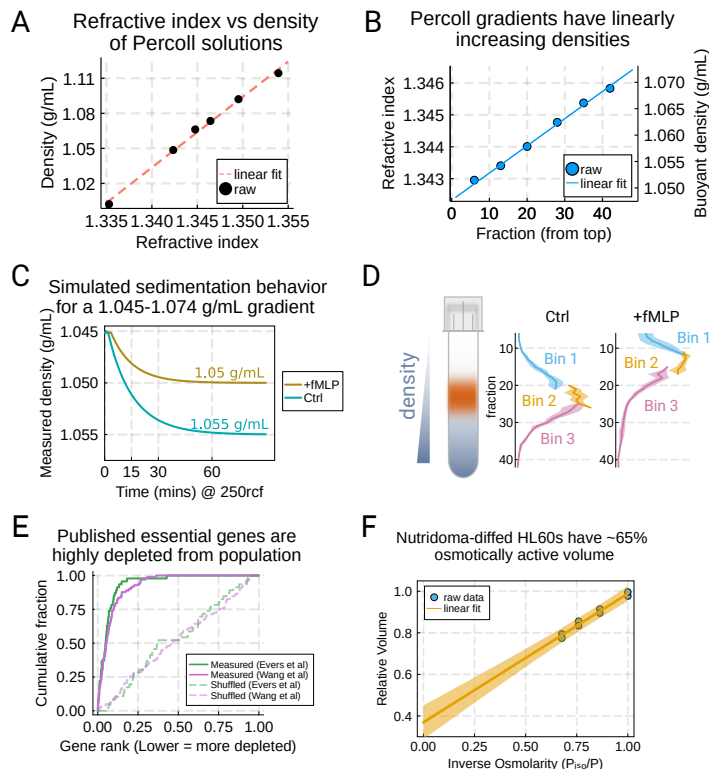


Figure 1.7: Validation of buoyant density assay

(A) Varying the amount of Percoll shows the linear relationship between the refractive index (as measured by a refractometer) and the density as determined by weighing solutions in a volumetric flask on an analytical balance. (B) Measuring the refractive index of different fractions from the gradient shows a high degree of linearity in buoyant density. (C) Simulation of the settling behavior of the control (teal) and stimulated cells (gold) in the Percoll gradients under a centrifugal force of 250 \times g. The cells are predicted to arrive at their isopycnic point after approximately one hour. (D) The binning strategy for the screen for the control (left) and stimulated (right) conditions. For each replicate of each condition, the cells were split across 6 different tubes and these were combined into 3 bins to balance the minimum number of cells per bin with the resolution gained from multiple bins. (E) Previously published essential genes from [11] and [51], in green and purple, respectively, were highly depleted from the population, validating functionality of our CRISPR-based knockout library. (F) Ponders relation for dHL-60s in suspension. Increasing amounts of hyperosmolarity drives the osmotically active fraction of the volume out of the cell, and projecting out to infinite osmolarity gives 65% of the cell volume as osmotically active.

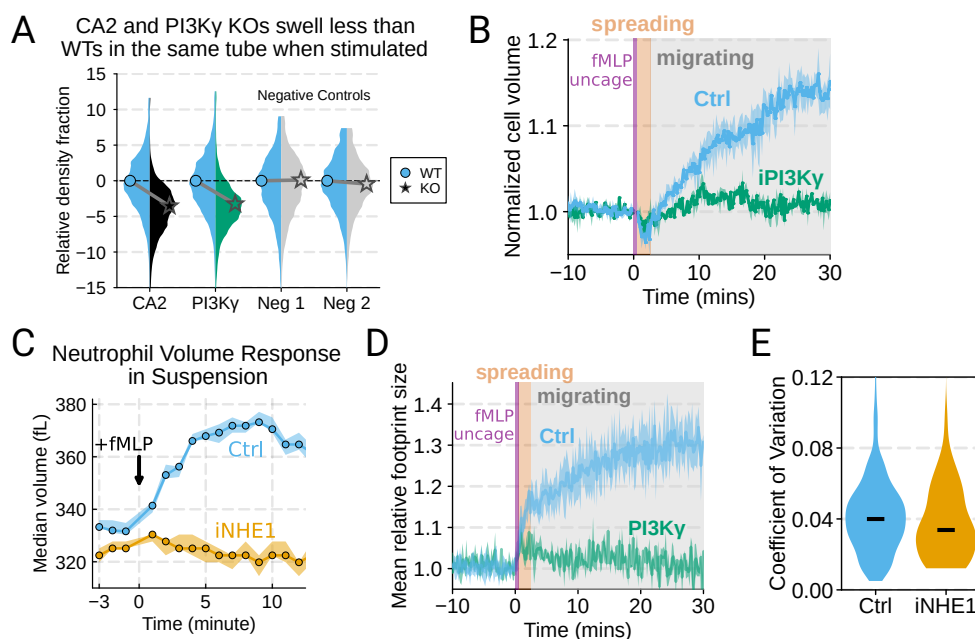


Figure 1.8: Additional validation of swelling screen hits

(A) Mixed WT and CRISPR KO dHL-60 populations post-stimulation show that CA2 (black) and PI3Ky (green) KO both fail to decrease their densities as much as the WT (cyan) population following chemoattractant stimulation. Cells with negative control guides (light grey) have normal volume responses. (B) PI3K/ inhibition completely blocks the chemoattractant-induced volume change in primary human neutrophils. (C) To validate the FxM results, primary human neutrophils were stimulated in suspension, and their volumes were measured using a Coulter counter (WT replicates = 4, NHE1 = 2). 20 nM fMLP was added at the 0 minute marker. (D) PI3K/ inhibition blocked the chemoattractant-drive shape change in human primary neutrophils, as measured by the change in footprint area in FxM (E) The coefficient of variation in volume for control (cyan) and iNHE1 (gold) human primary neutrophils undergoing chemokinesis are comparable, suggesting that the volume fluctuations are unchanged upon NHE1 inhibition despite the different baseline volumes.

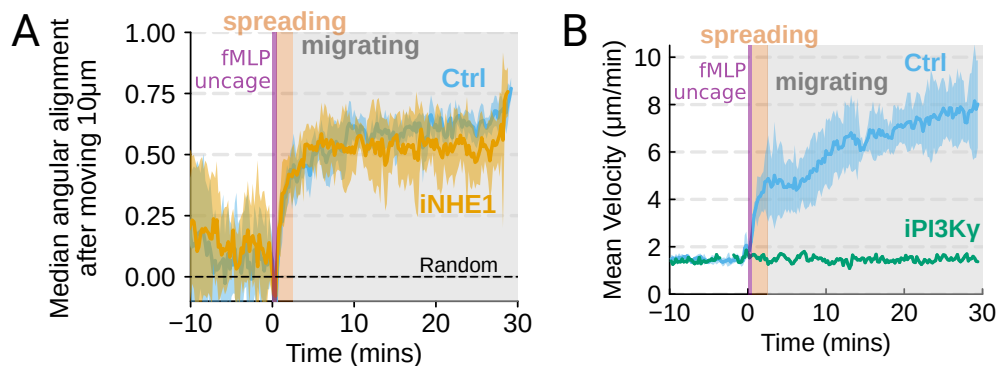


Figure 1.9: Additional validation of motility phenotypes

(A) Control neutrophils show an increased angular alignment upon stimulation as their motility becomes directional. NHE1-inhibition has very little effect on this process. (B) PI3K/ completely blocked the chemoattractant-induced motility increase in primary human neutrophils

Bibliography

- [1] Daniel B Allan et al. *soft-matter/trackpy: Trackpy v0.5.0*. Apr. 2021.
- [2] Jeff Bezanson et al. “Julia: A Fresh Approach to Numerical Computing”. In: *SIAM Rev.* 59.1 (Jan. 2017), pp. 65–98.
- [3] Jérôme Boulanger et al. “Patch-based nonlocal functional for denoising fluorescence microscopy image sequences”. en. In: *IEEE Trans. Med. Imaging* 29.2 (Feb. 2010), pp. 442–454.
- [4] C Cadart et al. “Chapter 6 - Fluorescence eXclusion Measurement of volume in live cells”. In: *Methods in Cell Biology*. Ed. by Thomas Lecuit. Vol. 139. Academic Press, 2017, pp. 103–120.
- [5] Sean R Collins et al. “Using light to shape chemical gradients for parallel and automated analysis of chemotaxis”. en. In: *Mol. Syst. Biol.* 11.4 (Apr. 2015), p. 804.
- [6] Fabienne Coury et al. “SLC4A2-mediated Cl⁻/HCO₃⁻ exchange activity is essential for calpain-dependent regulation of the actin cytoskeleton in osteoclasts”. en. In: *Proc. Natl. Acad. Sci. U. S. A.* 110.6 (Feb. 2013), pp. 2163–2168.

- [7] S Denk et al. “Complement C5a-Induced Changes in Neutrophil Morphology During Inflammation”. en. In: *Scand. J. Immunol.* 86.3 (Sept. 2017), pp. 143–155.
- [8] Sheryl P Denker and Diane L Barber. “Cell migration requires both ion translocation and cytoskeletal anchoring by the Na-H exchanger NHE1”. en. In: *J. Cell Biol.* 159.6 (Dec. 2002), pp. 1087–1096.
- [9] Peter Devreotes and Alan Rick Horwitz. “Signaling networks that regulate cell migration”. en. In: *Cold Spring Harb. Perspect. Biol.* 7.8 (Aug. 2015), a005959.
- [10] Arthur D Edelstein et al. “Advanced methods of microscope control using μ Manager software”. en. In: *J Biol Methods* 1.2 (2014).
- [11] Bastiaan Evers et al. “CRISPR knockout screening outperforms shRNA and CRISPRi in identifying essential genes”. en. In: *Nat. Biotechnol.* 34.6 (June 2016), pp. 631–633.
- [12] G John Ferguson et al. “PI(3)Kgamma has an important context-dependent role in neutrophil chemokinesis”. en. In: *Nat. Cell Biol.* 9.1 (Jan. 2007), pp. 86–91.
- [13] Christian Frantz et al. “Positive feedback between Cdc42 activity and H⁺ efflux by the Na-H exchanger NHE1 for polarity of migrating cells”. en. In: *J. Cell Biol.* 179.3 (Nov. 2007), pp. 403–410.
- [14] Juan Manuel Garca-Arcos et al. “Advected percolation in the actomyosin cortex drives amoeboid cell motility”. en. July 2022.

- [15] Brian R Graziano et al. “A module for Rac temporal signal integration revealed with optogenetics”. en. In: *J. Cell Biol.* 216.8 (Aug. 2017), pp. 2515–2531.
- [16] Brian R Graziano et al. “Cell confinement reveals a branched-actin independent circuit for neutrophil polarity”. en. In: *PLoS Biol.* 17.10 (Oct. 2019), e3000457.
- [17] S Grinstein, W Furuya, and E J Cragoe Jr. “Volume changes in activated human neutrophils: the role of Na⁺/H⁺ exchange”. en. In: *J. Cell. Physiol.* 128.1 (July 1986), pp. 33–40.
- [18] William H Grover et al. “Measuring single-cell density”. en. In: *Proc. Natl. Acad. Sci. U. S. A.* 108.27 (July 2011), pp. 10992–10996.
- [19] Hisayoshi Hayashi et al. “Na⁺/H⁺ exchange and pH regulation in the control of neutrophil chemokinesis and chemotaxis”. en. In: *Am. J. Physiol. Cell Physiol.* 294.2 (Feb. 2008), pp. C526–34.
- [20] Else K Hoffmann, Ian H Lambert, and Stine F Pedersen. “Physiology of Cell Volume Regulation in Vertebrates”. In: *Physiol. Rev.* 89.1 (Jan. 2009), pp. 193–277.
- [21] Andrew R Houk et al. “Membrane tension maintains cell polarity by confining signals to the leading edge during neutrophil migration”. en. In: *Cell* 148.1-2 (Jan. 2012), pp. 175–188.
- [22] John D Huber et al. “Identification of a potent sodium hydrogen exchanger isoform 1 (NHE1) inhibitor with a suitable profile for chronic dosing and demonstrated cardio-

- protective effects in a preclinical model of myocardial infarction in the rat”. en. In: *J. Med. Chem.* 55.16 (Aug. 2012), pp. 7114–7140.
- [23] Kinneret Keren et al. “Mechanism of shape determination in motile cells”. en. In: *Nature* 453.7194 (May 2008), pp. 475–480.
- [24] M Klein et al. “Polarization of Na(+)/H(+) and Cl(-)/HCO₃(-) exchangers in migrating renal epithelial cells”. en. In: *J. Gen. Physiol.* 115.5 (May 2000), pp. 599–608.
- [25] Tim Lämmermann et al. “Neutrophil swarms require LTB₄ and integrins at sites of cell death in vivo”. en. In: *Nature* 498.7454 (June 2013), pp. 371–375.
- [26] Wei Li et al. “MAGeCK enables robust identification of essential genes from genome-scale CRISPR/Cas9 knockout screens”. en. In: *Genome Biol.* 15.12 (Dec. 2014), pp. 1–12.
- [27] Xiuju Li et al. “A novel carbonic anhydrase II binding site regulates NHE1 activity”. en. In: *Biochemistry* 45.7 (Feb. 2006), pp. 2414–2424.
- [28] Xiuju Li et al. “Carbonic anhydrase II binds to and enhances activity of the Na⁺/H⁺ exchanger”. en. In: *J. Biol. Chem.* 277.39 (Sept. 2002), pp. 36085–36091.
- [29] Kayleigh J S Martin et al. “The role of phosphoinositide 3-kinases in neutrophil migration in 3D collagen gels”. en. In: *PLoS One* 10.2 (Feb. 2015), e0116250.

- [30] Mieke Metzemaekers, Mieke Gouwy, and Paul Proost. “Neutrophil chemoattractant receptors in health and disease: double-edged swords”. en. In: *Cell. Mol. Immunol.* 17.5 (May 2020), pp. 433–450.
- [31] Michael J Mitchell and Michael R King. “Shear-induced resistance to neutrophil activation via the formyl peptide receptor”. en. In: *Biophys. J.* 102.8 (Apr. 2012), pp. 1804–1814.
- [32] T J Mitchison, G T Charras, and L Mahadevan. “Implications of a poroelastic cytoplasm for the dynamics of animal cell shape”. en. In: *Semin. Cell Dev. Biol.* 19.3 (June 2008), pp. 215–223.
- [33] Tamas Nagy and Martin Kampmann. “CRISPulator: a discrete simulation tool for pooled genetic screens”. en. In: *BMC Bioinformatics* 18.1 (July 2017), p. 347.
- [34] P Novick, C Field, and R Schekman. “Identification of 23 complementation groups required for post-translational events in the yeast secretory pathway”. en. In: *Cell* 21.1 (Aug. 1980), pp. 205–215.
- [35] P Novick and R Schekman. “Secretion and cell-surface growth are blocked in a temperature-sensitive mutant of *Saccharomyces cerevisiae*”. en. In: *Proc. Natl. Acad. Sci. U. S. A.* 76.4 (Apr. 1979), pp. 1858–1862.
- [36] Marius Pachitariu and Carsen Stringer. “Cellpose 2.0: how to train your own model”. en. In: *Nat. Methods* 19.12 (Dec. 2022), pp. 1634–1641.

- [37] S O Pember et al. “Density heterogeneity of neutrophilic polymorphonuclear leukocytes: gradient fractionation and relationship to chemotactic stimulation”. en. In: *Blood* 61.6 (June 1983), pp. 1105–1115.
- [38] Esther Rincón, Briana L Rocha-Gregg, and Sean R Collins. “A map of gene expression in neutrophil-like cell lines”. en. In: *BMC Genomics* 19.1 (Aug. 2018), p. 573.
- [39] M Ritter et al. “Effect of inhibitors of Na^+/H^+ -exchange and gastric H^+/K^+ ATPase on cell volume, intracellular pH and migration of human polymorphonuclear leukocytes”. en. In: *Br. J. Pharmacol.* 124.4 (June 1998), pp. 627–638.
- [40] S Rosengren, P M Henson, and G S Worthen. “Migration-associated volume changes in neutrophils facilitate the migratory process in vitro”. en. In: *Am. J. Physiol.* 267.6 Pt 1 (Dec. 1994), pp. C1623–32.
- [41] Anand Rotte et al. “Effect of bacterial lipopolysaccharide on Na^+/H^+ exchanger activity in dendritic cells”. en. In: *Cell. Physiol. Biochem.* 26.4-5 (Oct. 2010), pp. 553–562.
- [42] Suvrajit Saha, Jason P Town, and Orion D Weiner. “Mechanosensitive mTORC2 independently coordinates leading and trailing edge polarity programs during neutrophil migration”. en. In: *Mol. Biol. Cell* 34.5 (May 2023), ar35.
- [43] Kheya Sengupta et al. “Spreading of neutrophils: from activation to migration”. en. In: *Biophys. J.* 91.12 (Dec. 2006), pp. 4638–4648.

- [44] Ophir Shalem et al. “Genome-scale CRISPR-Cas9 knockout screening in human cells”. en. In: *Science* 343.6166 (Jan. 2014), pp. 84–87.
- [45] Yejie Shi et al. “Stimulation of Na(+)/H(+) exchanger isoform 1 promotes microglial migration”. en. In: *PLoS One* 8.8 (Aug. 2013), e74201.
- [46] S I Simon, J D Chambers, and L A Sklar. “Flow cytometric analysis and modeling of cell-cell adhesive interactions: the neutrophil as a model”. en. In: *J. Cell Biol.* 111.6 Pt 1 (Dec. 1990), pp. 2747–2756.
- [47] Kimberly M Stroka et al. “Water permeation drives tumor cell migration in confined microenvironments”. en. In: *Cell* 157.3 (Apr. 2014), pp. 611–623.
- [48] Eliska Svastova et al. “Carbonic Anhydrase IX Interacts with Bicarbonate Transporters in Lamellipodia and Increases Cell Migration via Its Catalytic Domain*,” in: *J. Biol. Chem.* 287.5 (Jan. 2012), pp. 3392–3402.
- [49] Lorena A Vargas et al. “Inhibition of carbonic anhydrase prevents the Na⁺/H⁺ exchanger 1-dependent slow force response to rat myocardial stretch”. In: *American Journal of Physiology-Heart and Circulatory Physiology* 305.2 (July 2013), H228–H237.
- [50] Larisa Venkova et al. “A mechano-osmotic feedback couples cell volume to the rate of cell deformation”. en. In: *Elife* 11 (Apr. 2022).
- [51] Tim Wang et al. “Identification and characterization of essential genes in the human genome”. en. In: *Science* 350.6264 (Nov. 2015), pp. 1096–1101.

- [52] O D Weiner et al. “Spatial control of actin polymerization during neutrophil chemotaxis”. en. In: *Nat. Cell Biol.* 1.2 (June 1999), pp. 75–81.
- [53] David G Winkler et al. “PI3K- δ and PI3K- γ inhibition by IPI-145 abrogates immune responses and suppresses activity in autoimmune and inflammatory disease models”. en. In: *Chem. Biol.* 20.11 (Nov. 2013), pp. 1364–1374.
- [54] Yuqi Zhang et al. “Polarized NHE1 and SWELL1 regulate migration direction, efficiency and metastasis”. en. In: *Nat. Commun.* 13.1 (Oct. 2022), pp. 1–17.
- [55] Ewa Zlotek-Zlotkiewicz et al. “Optical volume and mass measurements show that mammalian cells swell during mitosis”. In: *J. Cell Biol.* 211.4 (Nov. 2015), pp. 765–774.

Publishing Agreement

It is the policy of the University to encourage open access and broad distribution of all theses, dissertations, and manuscripts. The Graduate Division will facilitate the distribution of UCSF theses, dissertations, and manuscripts to the UCSF Library for open access and distribution. UCSF will make such theses, dissertations, and manuscripts accessible to the public and will take reasonable steps to preserve these works in perpetuity.

I hereby grant the non-exclusive, perpetual right to The Regents of the University of California to reproduce, publicly display, distribute, preserve, and publish copies of my thesis, dissertation, or manuscript in any form or media, now existing or later derived, including access online for teaching, research, and public service purposes.

DocuSigned by:

Tamas Nagy

A9BC53336B72480...

Author Signature

5/20/2023

Date